Recovery of Image Blocks Using the Method of Alternating Projections

Jiho Park, *Member, IEEE*, Dong-Chul Park, *Senior Member, IEEE*, Robert J. Marks, II, *Fellow, IEEE*, and
Mohamed A. El-Sharkawi, *Fellow, IEEE*

Abstract—A technique for block-loss restoration in block-based image and video coding, dubbed *recovery of image blocks using the method of alternating projections* (RIBMAP), is developed. The algorithm is based on orthogonal projections onto constraint sets in a Hilbert space. For the recovery of a linear dimension N size block, a total of $8N$ vectors are extracted from the surrounding area of an $N \times N$ missing block. These vectors form a library from which the best matching spatial information for the missing block is extracted. Recovery vectors, including both undamaged and restored damaged pixels, are introduced. The vectors are used to find highly correlated information relating to the lost pixels. To assure continuity with the surrounding undamaged area, three additional convex constraints are formulated. Adherance to these sets is imposed using alternating projections. Simulation results using orthogonal projections demonstrate that RIBMAP recovers spatial structure faithfully. Simulation comparisons with other procedures are presented: Ancis and Giusto's hybrid edge-based average-median interpolation technique, Sun and Kwok's projections onto convex sets-based method, Hemami and Meng's interblock correlation interpolation approach, Shirani *et al.*'s modified interblock correlation interpolation scheme, and Alkachouh and Bellanger's fast discrete cosine transformation-based spatial domain interpolation algorithm. Characteristic of the results are those of the "Lena" JPEG image when one fourth of periodically spaced blocks in the image have errors. The *peak signal-to-noise ratio* of the restored image is 28.68, 29.99, 31.86, 31.69, 31.57, and 34.65 dB using that of Ancis and Giusto, Sun and Kwok, Hemami and Meng, Shirani *et al.*, Alkachouh and Bellanger, and RIPMAP, respectively.

Index Terms—Alternating projections, block-loss recovery, error concealment, image and video transmission, JPEG, MPEG, projections onto convex sets (POCS), projections.

I. INTRODUCTION

MANY compression transform codings, such as JPEG and MPEG standards, are based on block coding techniques using pixel block segmentation, motion estimation, *discrete cosine transformation* (DCT), and vector quantization [1]–[3]. When a block is lost, it can be estimated using adjacent pixels in post processing. *Recovery of image blocks using the method of alternating projections* (RIBMAP) is an effective way to do so.

Many spatial interpolation techniques for restoring missing blocks of received images have been proposed [4]. Wang *et al.* [5] present an optimization technique that recovers damaged blocks by minimizing the differences between the blocks and boundaries. Smooth images result. Park *et al.* [6] suggest a special case of [5] requiring a lower computational load while providing similar performance by imposing a smoothness constraint on the boundary and surrounding pixels of the missing blocks. Lee *et al.* [7] introduce a block-recovery technique based on fuzzy-logic reasoning. Hemami and Meng [8] propose an image-reconstruction algorithm exploiting interblock correlation. Shirani *et al.* [9] modify Hemami and Meng's algorithm, using more weights in the interpolation equation and, thereby, obtain more reliable diagonal-edge restoration. A fast DCT-based spatial domain interpolation technique is reported by Alkachouh and Bellanger [10]. These algorithms are effective for restoration of smooth images void of high spatial frequencies. Sun and Kwok [11] suggest the use of a spatial interpolation algorithm using *projections onto convex sets* (POCS) [12]–[17]. The adopted smoothness assumption imposed by these otherwise innovative algorithms limits reliable restoration detail of images, such as edges and complex textures.

We present a spectrally robust interpolative image-restoration method based on projections onto convex sets and onto a line in Hilbert space defined by the best-matched adjacent $N \times N$ pixels. Convex sets are defined for the constraints of dynamic range and gradient and the structure of the surrounding area of the corrupted blocks. Vectors containing both known and missing pixels are projected onto the lines in Hilbert space and, then, alternatingly among the convex constraint sets. The algorithm enables restored blocks to sustain the spectral and edge structure of the surrounding blocks and, consequently, to have striking continuity with neighboring pixels.

II. LINE DETECTION AND VECTOR FORMING

Image condition for missing-pixel interpolation is illustrated in Fig. 1. In Fig. 1(a), a missing block, M, with its surrounding neighborhood, A, is shown. The orientation of edges in the adjacent surrounding neighborhood, A, is assumed to expand its structure to the missing block, M. The structure in the missing block is dictated by the orientation of lines and edges in the surrounding pixels. Vectors formed from surrounding pixels with their own spatial information are extracted from adjacent surrounding blocks A. To restore the missing block M, two recovery vectors—including correctly received pixels and estimated missing pixels—are formulated. The recovery direction is chosen in accordance to the orientation of adjacent lines and edges.
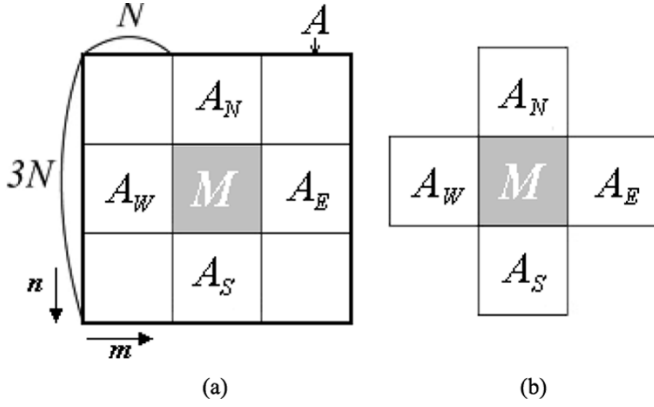
Fig. 1. Missing block (M) with surrounding neighborhood blocks of correctly received data. (a) Missing block M (in grey) and adjacent surrounding neighborhood A (in white). (b) Missing block M and four connected blocks A_E, A_W, A_N, and A_S.

A. Line Orientation Detection

A line detector in the spatial domain is applied to surrounding blocks to determine the line orientation of the area. The line masks L_v and L_h [see (1)] are applied to the surrounding blocks, A_E, A_W, A_N, and A_S in Fig. 1(b)

$$L_h = \begin{bmatrix} -1 & -1 & -1 \\ 2 & 2 & 2 \\ -1 & -1 & -1 \end{bmatrix} \quad L_v = \begin{bmatrix} -1 & 2 & -1 \\ -1 & 2 & -1 \\ -1 & 2 & -1 \end{bmatrix}. \quad (1)$$

Corresponding responses R_h and R_v at coordinates m, n are $R_h = 2 \cdot (x_{m,n-1} + x_{m,n} + x_{m,n+1}) - (x_{m-1,n-1} + x_{m-1,n} + x_{m-1,n+1} + x_{m+1,n-1} + x_{m+1,n} + x_{m+1,n+1})$ and $R_v = 2 \cdot (x_{m-1,n} + x_{m,n} + x_{m+1,n}) - (x_{m-1,n-1} + x_{m,n-1} + x_{m+1,n-1} + x_{m-1,n+1} + x_{m,n+1} + x_{m+1,n+1})$. The magnitude of responses R_h and R_v at all m, n coordinates in the four surrounding blocks (A_E, A_W, A_N, and A_S) are computed as

$$E_h = \sum_{A_E, A_W, A_N, A_S} |R_h|, \quad E_v = \sum_{A_E, A_W, A_N, A_S} |R_v|. \quad (2)$$

Edge orientation is determined by E_h and E_v. If E_h is larger than E_v, the missing block is considered a horizontal line-dominating block. Otherwise, it is considered a vertical line-dominating block. Lee *et al.* [7] and Sun and Kwok [11] adopt a similar edge-orientation detection using Sobel masks.

B. Surrounding Vectors

Since the surrounding neighborhood of a missing block is assumed to have spatial and spectral similarity with the missing pixels, the neighborhood area can be segmented into several pixel blocks, each of which has its own spatial and spectral characteristics. The segmentation of the neighborhood area and corresponding vectors are formed by shifting an $N \times N$ window on every grid of pixels in the surrounding neighborhood A in Fig. 1(a). This is illustrated in Fig. 2. The process yields an $N \times N$ vector $\mathbf{s}_k$ on that position. We, thereby, generate

$$\mathbf{s}_k = \{x : x(m,n), (m,n) \in B\} \quad (3)$$

where B is an $N \times N$ window in A, m and n are pixel indices, and k is an vector index. The number of the surrounding vectors $\mathbf{s}_k$ is $8N$, and k can be enumerated from 1 to $8N$ clockwise starting at the top-left corner, as shown in Fig. 2. Note that
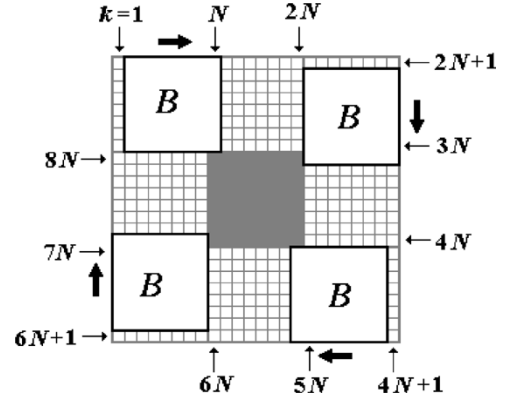
Fig. 2. Missing block with surrounding neighborhood and $N \times N$ window B to make the surrounding vector $\mathbf{s}_i$.

the window B cannot position outside the surrounding neighborhood area A. The number of surrounding vectors in a JPEG coding scheme is 64, and, in the case of MPEG, is it 128. If we define an $N \times N$ vector, $\mathbf{S}_k$ for $1 \leq k \leq 8N$, which is the two-dimensional (2-D) DCT pair of the surrounding vector s_k, then

$$\mathbf{S}_k = \mathbf{T} \cdot \mathbf{s}_k \text{ for } 1 \leq k \leq 8N \quad (4)$$

where $\mathbf{T}$ is 2-D DCT kernel.

C. Recovery Vectors

To restore a missing block, recovery vectors $\{\mathbf{r}_k | k = 1, 2\}$ are introduced. As shown in Fig. 3, according to the dominating line orientations in the surrounding blocks, two positions of the recovery vectors are employed. The position of recovery windows in Fig. 3(a) are for the vertical line-dominating area, while those in Fig. 3(b) are for the horizontal line-dominating area. In each case, two $N \times N$ recovery pixel vectors are formed from the windows, and each vector includes $(N-1) \times N$ known and $1 \times N$ unknown or $N \times (N-1)$ known and $N \times 1$ unknown pixels. This is shown in Fig. 3. The gray in the windows indicates missing pixels, while the white-colored portion indicates correctly received pixels. We, thereby, generate

$$\mathbf{r}_k = \{x : x(m,n), (m,n) \in C\} \quad (5)$$

where C is an $N \times N$ window in A (for surrounding blocks) and M (for the missing block), m and n are pixel indices, and k is a vector index. Let the $N \times N$ vector, $\mathbf{R}_k$ for $1 \leq k \leq 2$, be the 2-D DCT pair of the surrounding vector, $\mathbf{r}_k$

$$\mathbf{R}_k = \mathbf{T} \cdot \mathbf{r}_k \text{ for } 1 \leq k \leq 2. \quad (6)$$

After missing pixels in a recovery vector are restored, recovery windows slide in opposite directions to each other to extract a new recovery vector to restore the next N missing pixels. This is shown by the arrows in Fig. 3. The methods of Lee *et al.* [7] and Tselkeridon and Pitas [19] also use a sliding recovery window for lost pixel restoration. RIBMAP is different from these in that windows in [7] move diagonally using different sizes at different times. Windows in RIBMAP move vertically or horizontally according to line orientation in the surrounding area and include $1 \times N$ missing pixels at any time. Furthermore, missing pixels in [7] are restored by cubic spline interpolation/extrapolation and fuzzy reasoning, while missing
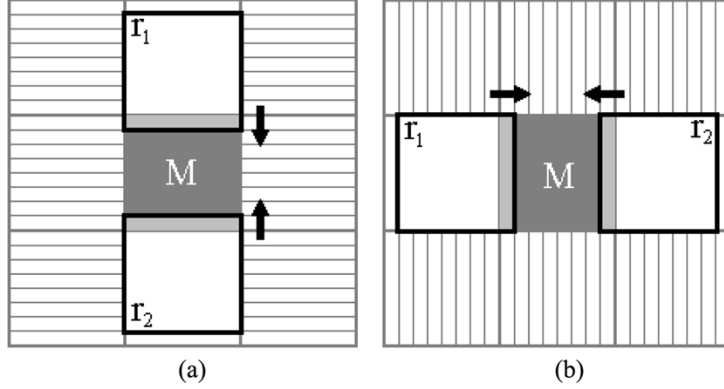
Fig. 3. Missing block with surrounding neighborhood and two $N \times N$ recovery vectors $\mathbf{r}_i$. (a) Recovery vectors $\mathbf{r}_i$ for the vertical line-dominating area. (b) Recovery vectors $\mathbf{r}_i$ for the horizontal line-dominating area.
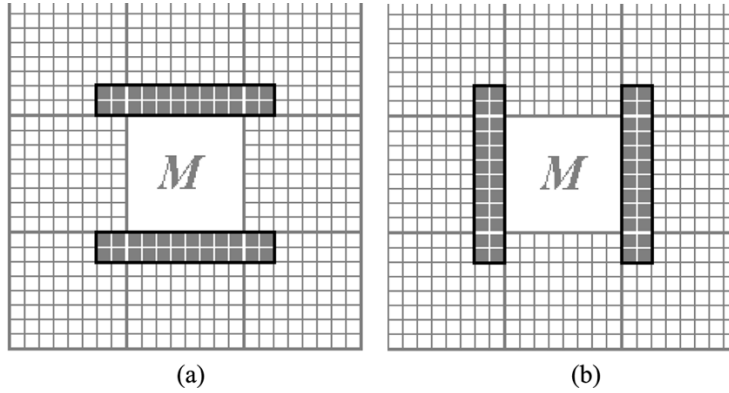
Fig. 4. Areas for computing parameters α_1 and α_2. Upper and lower blocks in (a) are areas to compute α_1 and α_2, respectively. The left and right blocks in (b) are areas for α_1 and α_2, respectively. Pictured here are (a) the area for computing parameter α_i in the vertical line-dominating area and (b) the area for computing parameter α_i in the horizontal line-dominating area.

pixels in RIBMAP are restored by projections. In the algorithm [19], 4×4 windows slide on a missing block between the 4×4 blocks of the "best match" in upper and lower surrounding neighborhoods of a missing block for macroblock recovery on MPEG-2.

III. RESTORATION ALGORITHM USING THE METHOD OF PROJECTIONS

In this section, a projection-based signal-restoration technique is developed. Projection operators and convex constraint sets are formulated to facilitate recovery of missing pixels using recovery vectors $\{\mathbf{r}_i | i = 1, 2\}$. To assure continuity, convex sets in the algorithm are specified by the area surrounding the missing block. Recovery vectors are alternately projected onto a line in a Hilbert space defined by the best matched adjacent $N \times N$ pixels and onto the convex sets. The missing pixels are, thereby, restored iteratively.

A. Projection Operators

1) Projection Operator P_1: The vectors $\{\mathbf{s}_j | 1 \leq j \leq 8N\}$, extracted from the surrounding blocks, A, are used to form a convex hull in an $N \times N$-dimensional space. Recovery vectors, $\{\mathbf{r}_i | i = 1, 2\}$, are then projected in the DCT domain onto the line between closest[1] vertex of the convex hull and the origin of the space.

[1]In the mean-square sense.

Let $\{\mathbf{r}_i | i = 1, 2\}$ and $\{\mathbf{s}_j | 1 \leq j \leq 8N\}$ be recovery and surrounding vectors, respectively. The surrounding vectors are used to form a convex hull. Each vector $\mathbf{s}_j$ becomes a vertex of the convex hull. The closest vertices $\{\hat{\mathbf{s}}_i = \mathbf{s}_{d_i} | i = 1, 2\}$ of the convex hull to the recovery vectors $\{\mathbf{r}_i | i = 1, 2\}$ are found in the mean-square sense

$$d_i = \arg\min_j \|\mathbf{r}_i - \mathbf{s}_j\| \quad \text{for } 1 \leq i \leq 2, \ 1 \leq j \leq 8N \quad (7)$$

or, equivalently[2]

$$d_i = \arg\min_j \|\mathbf{R}_i - \mathbf{S}_j\| \quad \text{for } 1 \leq i \leq 2, \ 1 \leq j \leq 8N \quad (8)$$

where $\mathbf{R}_i = \mathbf{T} \cdot \mathbf{r}_i$, $\mathbf{S}_j = \mathbf{T} \cdot \mathbf{s}_j$, and $\mathbf{T}$ is a 2-D DCT kernel. The recovery vectors in the DCT domain, $\{\mathbf{R}_i | i = 1, 2\}$ are then orthogonally projected onto the selected vertex $\hat{\mathbf{S}}_i$, as

$$P_{\hat{\mathbf{S}}_i}(\mathbf{R}_i) = \frac{\langle \mathbf{R}_i, \hat{\mathbf{S}}_i \rangle}{\|\hat{\mathbf{S}}_i\|^2} \cdot \hat{\mathbf{S}}_i \quad i = 1, 2 \quad (9)$$

where $\langle \cdot, \cdot \rangle$ is the inner product of two vectors and $\| \cdot \|$ is the ℓ_2 vector norm. Consequently, the projection operator P_1 translated to the DCT domain is

$$P_1 \cdot \mathbf{R}_i(u, v) = \begin{cases} P_{\hat{\mathbf{S}}_i}(\mathbf{R}_i(u, v)), & \text{for } u, v \neq 0 \\ \mathbf{R}_i(u, v), & \text{otherwise.} \end{cases} \quad (10)$$

To preserve the dc level, the dc value in the recovery vectors, $\{\mathbf{r}_i | i = 1, 2\}$, is not changed.

2) Projection Operator P_2: Projection operator P_2 imposes constraints on the range on the restored pixel values. It operates

[2]The 2-D DCT is an orthonormal transform and, hence, norm preserving.

Fig. 5.   Experiment on a lost block size of 8×8 pixels of the "Lena" image. (a) original, 512×512. (b) Damaged image of one missing block out of every four. Image restored using the methods of (c) Ancis and Giusto (PSNR $= 28.68$ dB). (d) Sun and Kwok (PSNR $= 29.99$ dB). (e) Hemami and Meng (PSNR $= 31.86$ dB). (f) Shirani *et al.* (PSNR $= 31.69$ dB). (g) Alkachouh and Bellanger (PSNR $= 31.57$ dB). (h) RIBMAP (PSNR $= 34.65$ dB).

in the spatial domain. The convex set C_2 for the projection operator P_2 is

$$C_2 = \{f : F_{\min} \leq f_n \leq F_{\max} \text{ for } n \in L\} \qquad (11)$$

where L is the set of missing pixels and $F_{\min}$ and $F_{\max}$ are chosen minimum and maximum intensities of an image, respec-

tively. The corresponding projection operator P_2 is a thresholding

$$P_2 \cdot f_n = \begin{cases} F_{\min}, & \text{for } f_n < F_{\min}, n \in L \\ F_{\max}, & \text{for } f_n > F_{\max}, n \in L \\ f_n, & \text{for } F_{\min} \leq f_n \leq F_{\max}, n \in L \\ c_n, & \text{otherwise} \end{cases} \qquad (12)$$
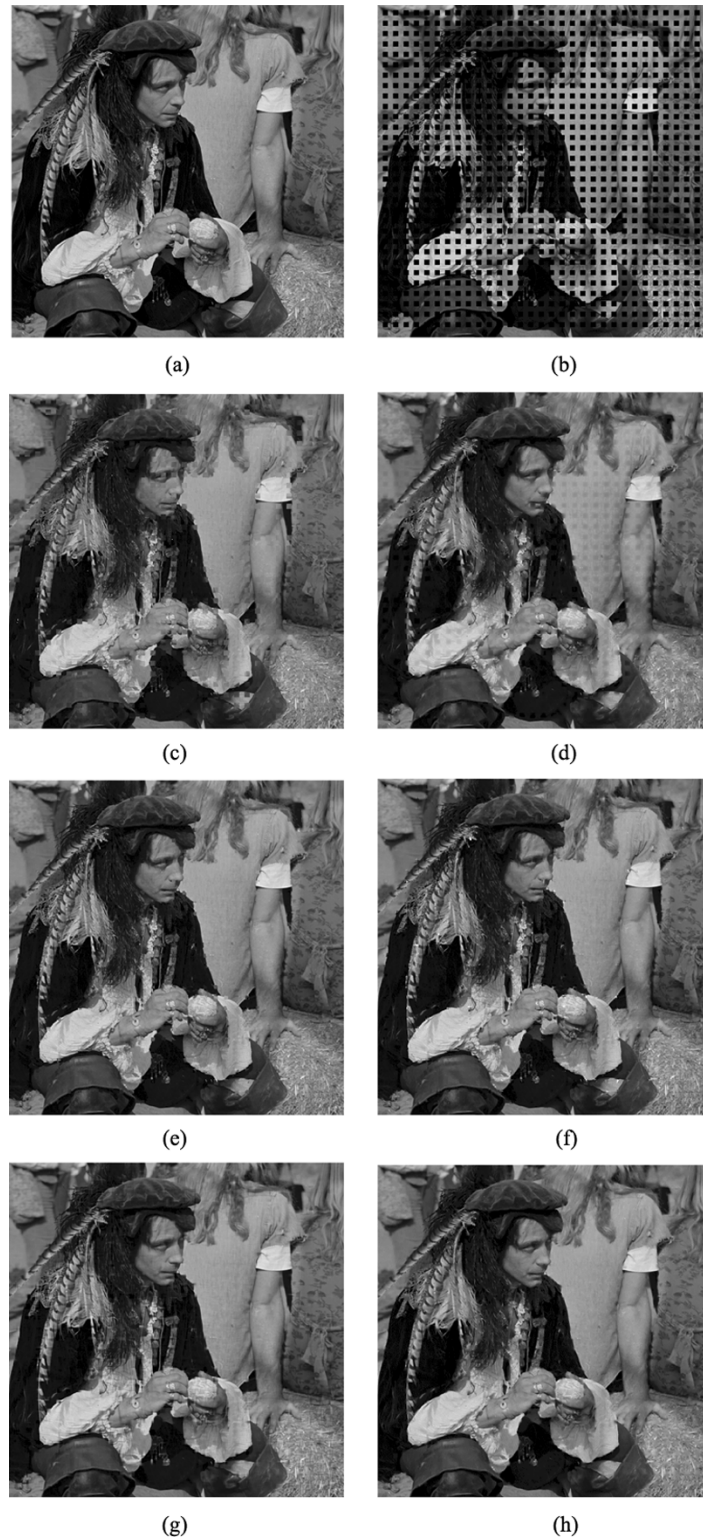
Fig. 6.   Experiment on a lost block size of 8×8 pixels of the "Masquerade" image. (a) Original 512×512. (b) Damaged image of one missing block out of every four. Restoration using the methods of (c) Ancis and Giusto (PSNR $= 25.47$ dB). (d) Sun and Kwok (PSNR $= 27.25$ dB). (e) Hemami and Meng (PSNR $= 27.65$ dB). (f) Shirani *et al.* (PSNR $= 27.44$ dB). (g) Alkachouh and Bellanger (PSNR $= 27.94$ dB). (h) RIBMAP (PSNR $= 29.87$ dB).

where n is the pixel index c_n is the known pixel value and L is the missing pixels of the recovery vectors.

3) Projection Operators P_3: A range constraint for continuity within the surroundings neighborhood of a restored block is imposed for smooth reconstruction of a damaged image. Yang *et al.* propose a projection-based spatially adaptive reconstruction of images [20], [21]. In Yang *et al.*'s algorithm, convex sets are developed for deblocking or capturing the smoothness properties of the desired image [20], [21]. The projection operator P_3 is similarly motivated.

TABLE I
PSNRs FOR "LENA," "MASQUERADE," "PEPPERS," "BOAT," "ELAINE," AND "COUPLE" FOR 8 × 8 PIXEL BLOCKS

	Lena	Masquerade	Peppers	Boat	Elaine	Couple	Average
Ancis and Giusto	28.68	25.47	27.92	26.33	29.84	28.24	27.75
Sun and Kwok	29.99	27.25	29.97	27.36	30.95	28.45	29.00
Hemami and Meng	31.86	27.65	31.83	29.36	32.07	30.31	30.51
Shirani *et al.*	31.69	27.44	31.72	29.22	32.10	30.34	30.42
Alkachouh and Bellanger	31.57	27.94	32.76	30.11	31.92	30.99	30.88
RIBMAP	34.65	29.87	34.20	30.78	34.63	31.49	32.60
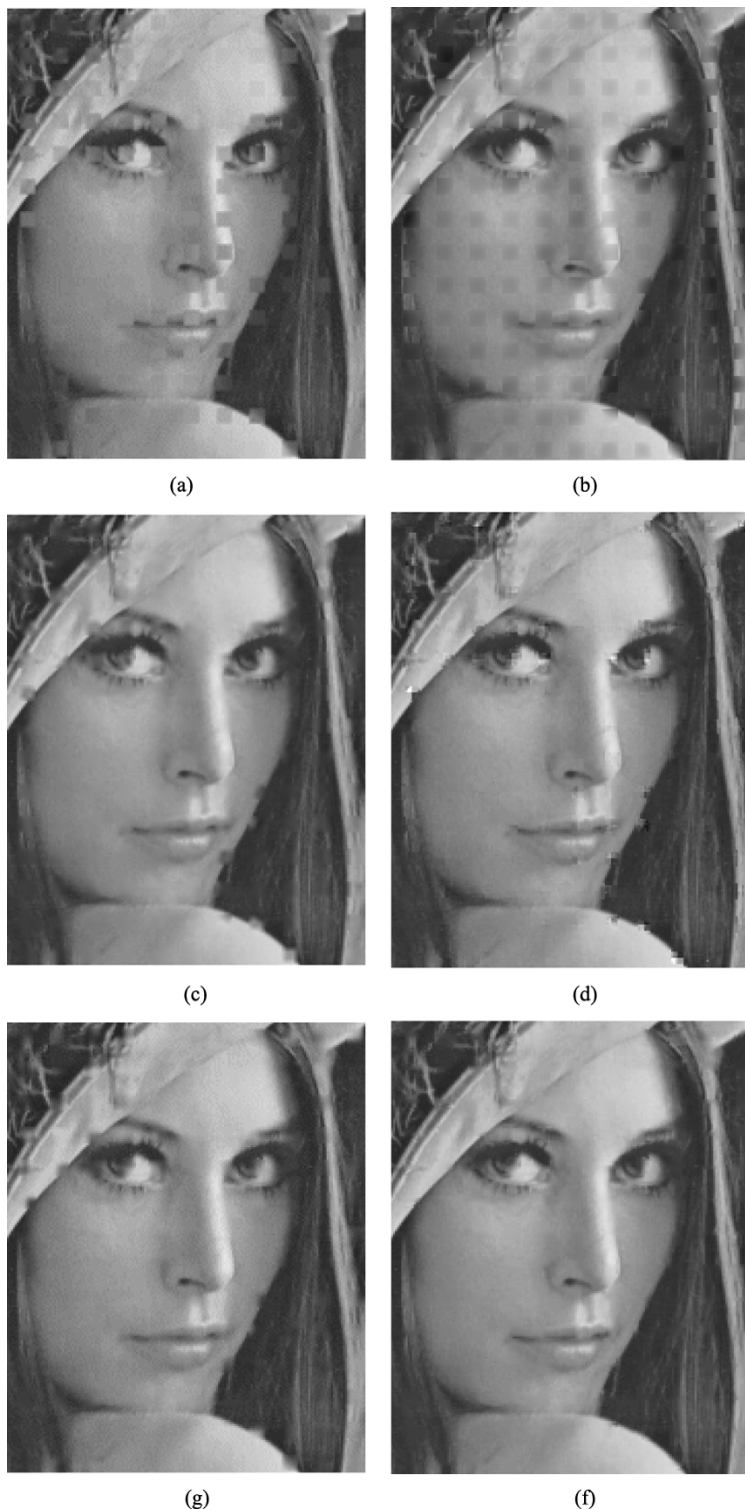
Fig. 7.   Potion of the magnified restored "Lena." (a) Ancis and Giusto. (b) Sun and Kwok. (c) Hemami and Meng. (d) Shirani *et al.* (e) Alkachouh and Bellanger. (f) RIBMAP.
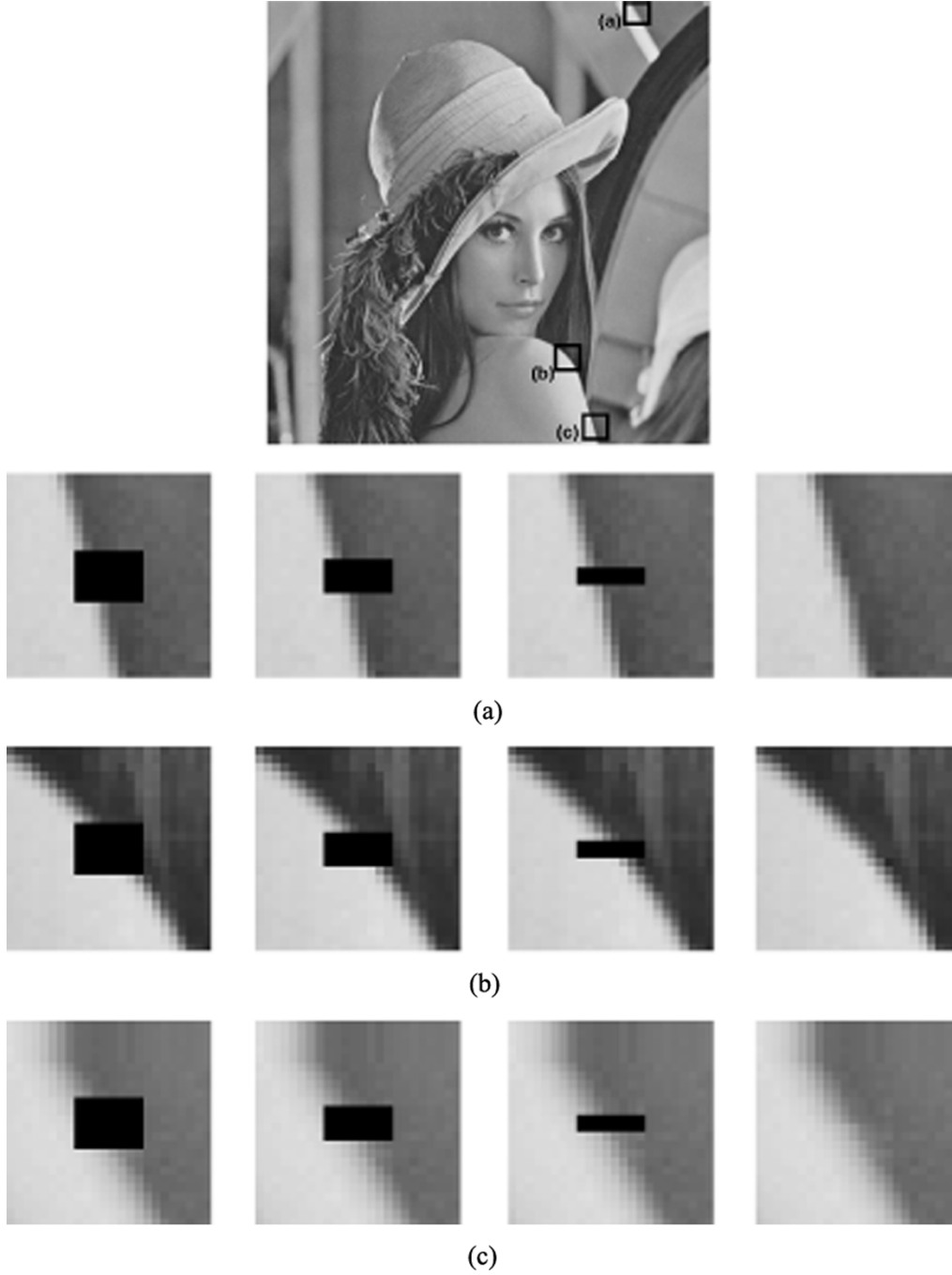
Fig. 8.   Restoration process for moving recovery vectors in RIBMAP. Steps are shown sequentially from the left image to the right. In each step, spatial structure in surrounding areas is used to estimate the structure of a missing block.

Let $\mathbf{f}$ be the vector of missing pixels in a recovery vector, $\mathbf{g}$ be the vector of adjacent pixels to the missing line in the same vector, and $\mathbf{h}$ be $N \times 1$ vector of $\mathbf{f} - \mathbf{g}$. Define $\mathbf{h} = [(f_0 - g_0), \ldots, (f_N - g_N)] = \mathbf{f} - \mathbf{g}$. By setting the vector $\mathbf{h}$ as a bounded signal with a constant, α, the convex set for the third projection operator P_3 can be obtained as

$$C_3 = \{\mathbf{h} : |h_n| \leq \alpha\} \qquad (13)$$

where n is the pixel index and α is a predetermined constant. The value of α can be set to the maximum value of differences

between pixels which are adjacent to the missing block in the surrounding neighborhood. Consequently, the projection operator P_3 is

$$P_3 \cdot f_n = \begin{cases} g_n - \alpha, & \text{for } h_n < -\alpha \\ g_n + \alpha, & \text{for } h_n > \alpha \\ f_n, & \text{otherwise} \end{cases} \qquad (14)$$

where $1 \leq n \leq N$. The projection operator P_3 limits the difference of adjacent known and missing-pixel values. The limitation allows the proposed algorithm to restore a damaged block

Fig. 9.   Experiment on a row of missing 8×8 blocks on the "Lena" image. (a) original 512×512. (b) Damaged image. (c) Image recovered by Hemami and Meng's method (PSNR $= 26.86$ dB). (d) Image recovered using RIBMAP (PSNR $= 30.18$ dB).

without reconstruction artifacts. It also makes the proposed algorithm applicable to a damaged block of diagonal edges even though the algorithm adopts only vertical or horizontal recovery directions.

4) Projection Operator P_4: After all pixels in a missing block are restored, a final convex constraint is applied to two center lines of the restored block to reduce variations due to use of different restoration directions. Assume $\mathbf{e}$ to be a $1 \times N$ vector of the differences between two center lines in a restored block such as $\mathbf{e} = [(f_{c1,0} - f_{c2,0}), \ldots, (f_{c1,N} - f_{c2,N})]$ where $\mathbf{f}_{c1}$ and $\mathbf{f}_{c2}$ are the final restored pixels of each center line in a restored block. By setting the vector $\mathbf{e}$ as a bounded signal with a predetermined constant β, the convex constraint C_4 and corresponding operator P_4 are obtained by

$$C_4 = \{\mathbf{e} : |e_n| \leq \beta\} \tag{15}$$

$$P_4 \cdot f_{m,n} = \begin{cases} \frac{(f_{c1,n} + f_{c2,n})}{2 \pm \beta}, & \text{for } h_n < -\beta \\ \frac{(f_{c1,n} + f_{c2,n})}{2 \mp \beta}, & \text{for } h_n > \beta \\ f_{m,n}, & \text{otherwise} \end{cases} \tag{16}$$

where m and n are the pixel indices and $\mathbf{f}_{c1}$ and $\mathbf{f}_{c2}$ are the vectors of missing pixels in two center lines of the recovery vectors. The projection P_4 is applied only in the final step and thus does not affect the convergence of alternating projections.

B. Iterative Algorithm for Pixel Interpolations

Missing pixels are restored iteratively by alternatingly projecting onto the specified constraint sets [12]. Specifically

$$f_{i+1} = P_1 \cdot P_2 \cdot P_3 \cdot f_i \tag{17}$$

where i is the iteration index, f_i is restored signal at iteration i, and P_j is the jth projection operator onto a line in Hilbert space $(j = 1)$ or onto convex sets C_j $(2 \leq j \leq 3)$. After all pixels in a missing block are restored, the projection operator P_4 is applied to the center lines of the block as described in the previous section. The computations required in the proposed algorithm are mainly a DCT, an inverse DCT, and projection operations in alternating projections. Here is the pseudocode.
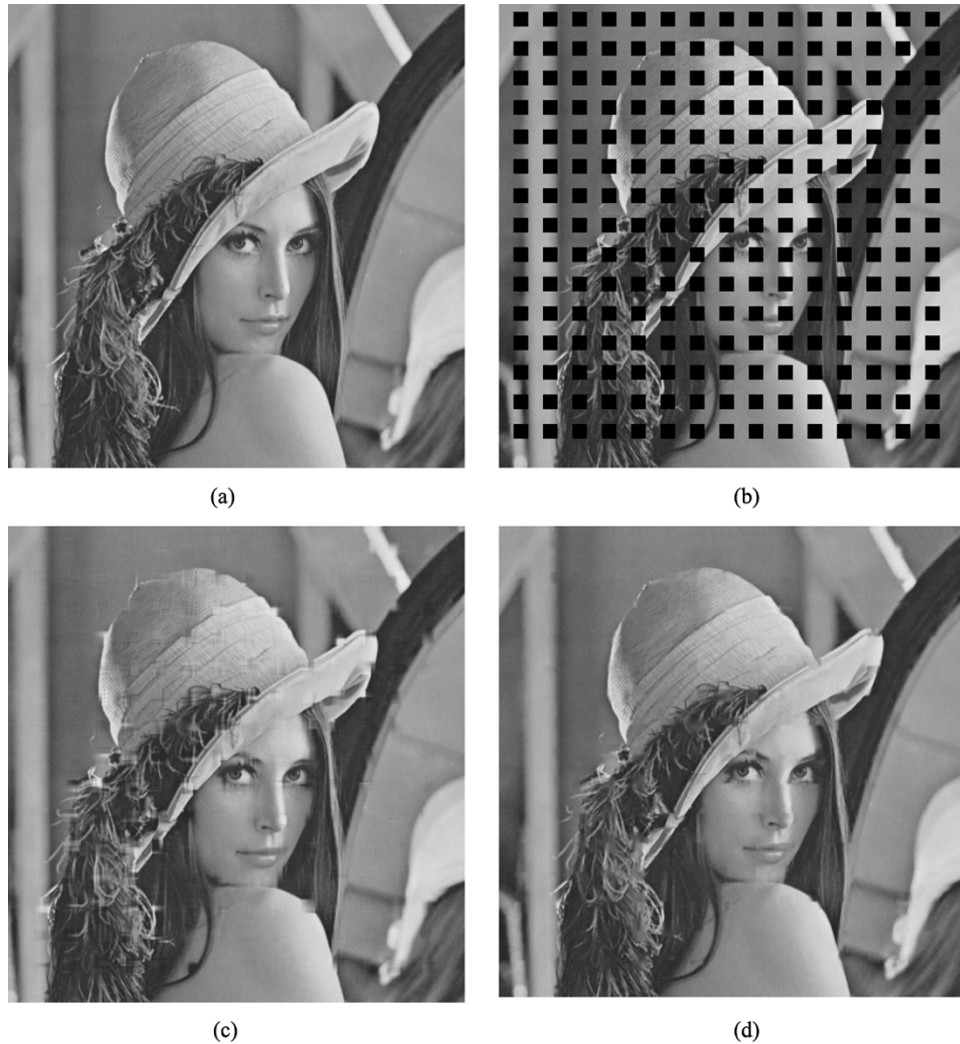
Fig. 10. Experiment on a lost block size of 16×16 pixels in the "Lena" image. (a) Original 512×512. (b) Damaged image with one missing block out of every four. (c) Image recovered by Alkachouh and Bellanger's method (PSNR $= 28.75$ dB). (d) Image recovered by RIBMAP (PSNR $= 32.708$ dB).

```
Algorithm
 compute gradients, T_h and T_v
 make surrounding vector library, s
 loop
  make recovery vectors, r_1 and r_2
  loop
   projection operator P_1
   projection operator P_2
   projection operator P_3
  endloop (iteratation == I)
 endloop (entire block restored == YES)
 projection operator P_4
End
```

IV. EXPERIMENTAL RESULTS

RIBMAP is tested on several 256 gray-level images. Results are compared with those of other block-recovery algorithms, such as the following: the hybrid edge-based average-median interpolation technique of Ancis and Giusto [22]; the POCS-based recovery technique by Sun and Kwok[3] [11]; the interblock correlation interpolation scheme of Hemami and Meng [8]; the modified interblock correlation interpolation scheme by Shirani *et al.* [9]; and the fast DCT-based spatial domain interpolation technique by Alkachouh and Bellanger [10].

Ancis and Giusto's algorithm involves average and average-median operations to interpolate each missing coefficient according to surrounding blocks edge presentation criteria. Hemami and Meng's algorithm finds four optimal weights using linear least squares. Spatial differences of four adjacent blocks are minimized to generate missing pixels using linear interpolation with the generated weights and the pixels in the same position in adjacent blocks. Shirani *et al.*'s algorithm uses eight weights, rather than four, to obtain better performance on diagonal-edge restoration. In Alkachouh and Bellanger's algorithm, missing block and border pixels are transformed using the DCT. High-frequency coefficients are set to zero. An inverse DCT yields the restoration.

[3]In Sun and Kwok's algorithm, smooth POCS restoration is tested and a low-pass filter radius $R_{th} = 3$ is applied as described in [11].
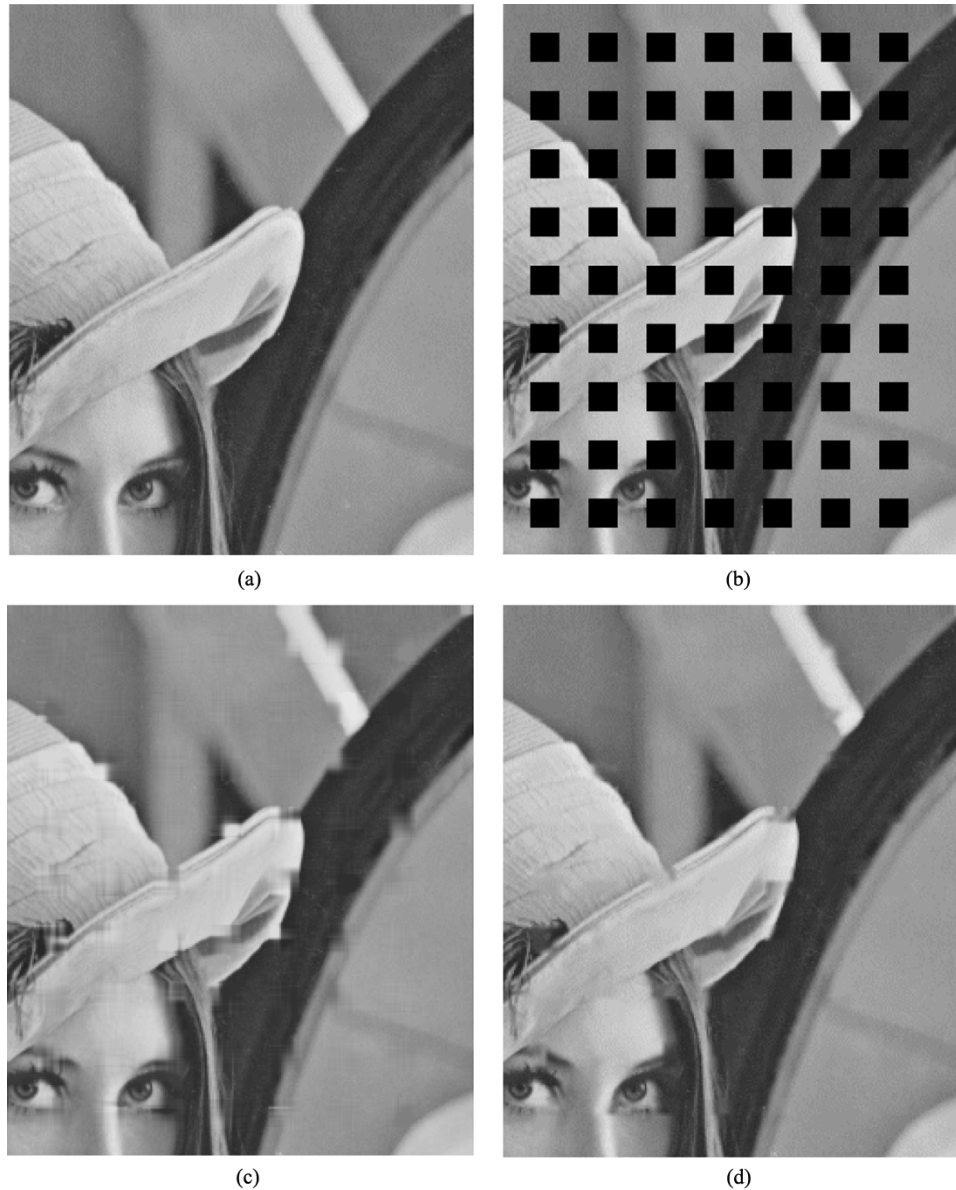
Fig. 11. Experiment on a lost block size of 16×16 pixels in the "Lena" image (enlarged). (a) Original 512×512. (b) Damaged image of one missing block out of every four. (c) Image recovered by Alkachouh and Bellanger's method. (d) Image recovered by RIBMAP.

Missing block sizes of 8×8 pixels are used for JPEG images and block sizes of 16×16 pixels are tested for intracoding of MPEGs. The size of the test images is 512×512 for "Lena," "Peppers," "Masquerade," "Boat," "Elaine," and "Couple." The size of "Foreman" is 176×144. An error is imposed on one fourth of the blocks with the assumption that macroblocks are interleaved on packing [23]. The number of iterations tested for the recovery of the missing row/column in each recovery vector of RIBMAP is set to 10.

Projections in RIBMAP do not always converge to one point, but the difference in solutions is typically negligible. Throughout the experiments, the initial point f_0 of the missing pixels of the recovery vectors $\mathbf{r}$ is set to the adjacent value of the known pixels in the same vector.

To determine the proper line orientation and recovery direction, line masks are applied on the neighborhood blocks A_E, A_W, A_S, and A_N as shown in Fig. 1(a) for the 8×8 pixel

block size and (b) on half the blocks for the 16×16 pixel block size. For the vertical line-dominating area, the parameter α for the projection operator P_3 is set to the maximum value of the difference between two adjacent pixels in the same column in the gray-colored blocks shown in Fig. 4(a). For the horizontal line-dominating area, α_k is set to the maximum value of the differences between two adjacent pixels in the same row shown as the gray-colored blocks in Fig. 4(b). In the case of Fig. 4(b), α is defined as

$$\alpha = \max |f(x,y) - f(x,y-1)|$$
$$x_0 - 2 < x < x_0 + N + 1,$$
$$y = y_0 - 1 \text{ or } y_0 + N + 1 \quad (18)$$

where (x_0, y_0) is the top-left pixel of a missing block M.

Simulation results on a missing block size of 8×8 pixels in the "Lena" and "Masquerade" images are shown in Figs. 5 and
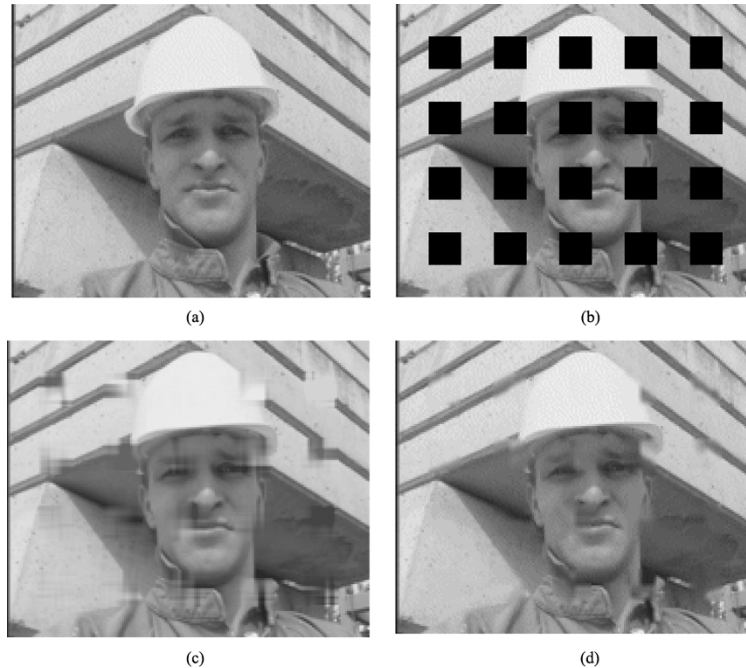
Fig. 12.   Experiment on a lost block size of 16×16 pixels in the first frame of the "Foreman" sequential images. (a) Original 144×176. (b) Damaged image of one missing block out of every four. (c) Image recovered by the method of Alkachouh and Bellanger (PSNR $= 25.65$ dB). (d) Image recovered by RIBMAP (PSNR $= 30.34$ dB).

6, respectively. The peak signal-to-noise ratio (PSNR) [24], used as a measure of the restored image quality, is given by

$$\text{PSNR} = 10 \cdot \log \left(\frac{N_1 \cdot N_2 \cdot 255^2}{\sum\limits_{m=1}^{N_1} \sum\limits_{n=1}^{N_2} |f(m,n) - \hat{f}(m,n)|^2} \right) \quad (19)$$

where f and $\hat{f}$ are the value of original and restored image of $N_1 \times N_2$ pixels, respectively.

Image (a) in Figs. 5 and 6 are originals, while image (b) in Figs. 5 and 6 are damaged. Image (c) in Figs. 5 and 6 show restored images by Ancis and Giusto's algorithm. The PSNR of (c) in Figs. 5 and 6 is 28.68 and 25.47 dB, respectively. Restored images by Sun and Kwok's algorithm are shown in (d) of Figs. 5 and 6, with PSNRs of 29.99 and 27.25 dB, respectively. Recovered images by Hememi and Meng's linear interpolation scheme and Shirani *et al.*'s algorithm are shown in (e) and (f) of Figs. 5 and 6, respectively. The PSNR of each image in (e) is 31.86 and 27.65 dB, and the PSNR in (f) is 31.69 and 27.44 dB, respectively. Restored images by Alkachouh and Bellanger's fast DCT-based spatial domain interpolation scheme are shown in (g) of Figs. 5 and 6, and its PSNR is 31.57 and 27.94 dB, respectively. In (f) of Figs. 5 and 6, images recovered by RIBMAP are shown. The PSNR of each image is 34.65 and 29.87 dB, respectively. In both objective and subjective comparisons, the qualities of recovered images by RIBMAP are the most favorable in all cases. Table I summarizes the PSNRs of the restored images in the case of 8×8 pixel block.

In Fig. 7, magnified portions of the restored "Lena" images are shown. Fig. 7(a)–(f) is restored using the methods of Ancis and Giusto, Sun and Kwok, Hemami and Meng, Shirani *et al.*,

Alkachouh and Bellanger, and RIBMAP, respectively. Images in Fig. 7 show that RIBMAP gives acceptable performances at edges such as the rim of the hat and the chin of the face, as well as in monotone areas such as face and shoulder. Fig. 8 shows restoration result for each sequential step. The spatial structure of surrounding area can be seen expanding into the missing block.

Simulation results on rows of missing blocks in "Lena" is shown in Fig. 9. Image (a) in Fig. 9 is the original while image (b) is damaged. Image (c) in Fig. 9 shows the damaged image restored using Hememi and Meng's linear interpolation scheme. The restoration PSNR is 26.86 dB. In this case, the first block of a missing row is first restored. Adjacent blocks are then restored sequentially as described in [8]. In (d) of Fig. 9, the image recovered using RIBMAP is shown. Only the vertical restoration direction and the available surrounding area are used for the restoration when RIBMAP is applied. The PSNR of the image is 30.18 dB.

For MPEG intracoding, a 16×16 macroblock missing case in used for "Lena." The first frame of "Foreman" is also used. In Figs. 10 and 12, test results on a block size of 16×16 pixels are shown. Image (a) in Figs. 10–12 are the original, and image (b) in Figs. 10–12 are the images with the missing pixels. Recovered images by Alkachouh and Bellanger's fast DCT-based spatial domain interpolation scheme are shown in (c) of Figs. 10–12, respectively. The PSNRs in (c) of Figs. 10 and 12 are 28.75 and 25.65 dB, respectively. In (d) of Figs. 10–12, images recovered by RIBMAP are shown. The PSNRs of each image in (d) of Figs. 10 and 12 are 32.70 and 30.34 dB, respectively. The images in Fig. 11 are enlarged versions of the top right of Fig. 10. Figs. 11(d) and 12 (d) show that RIBMAP restored edges, such as lines, in the background faithfully. Monotone regions are also restored faithfully.

(a)

(b)
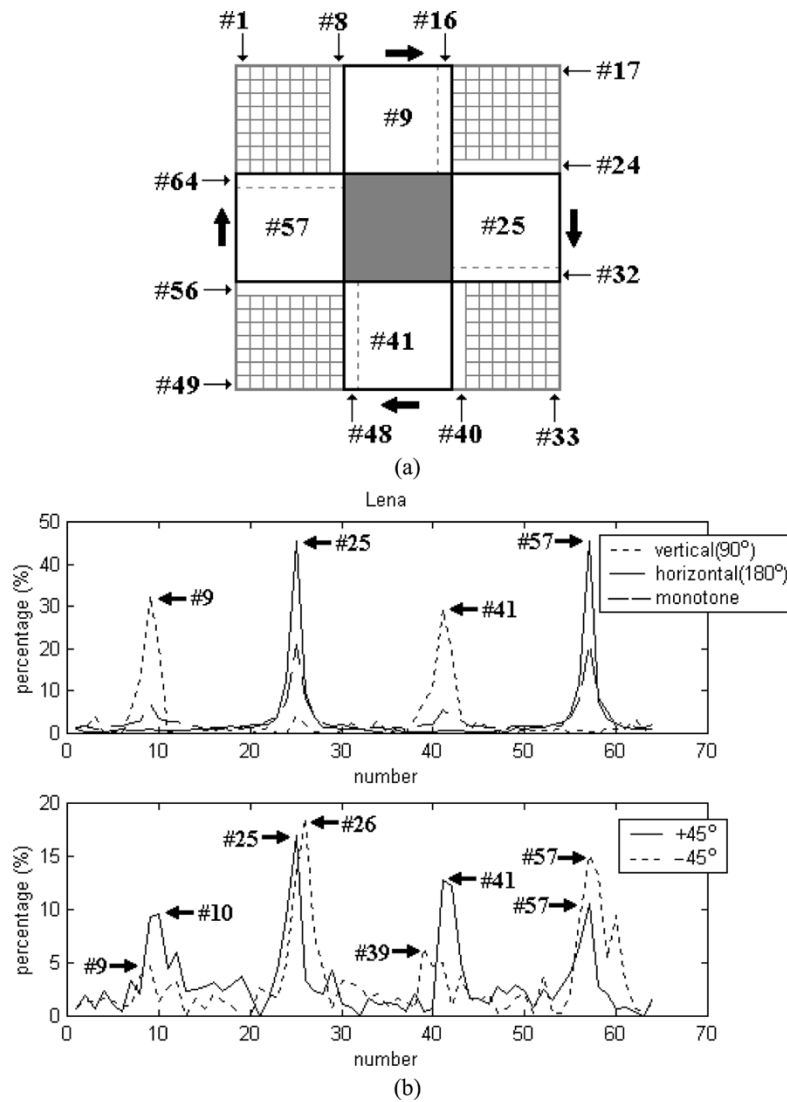
Fig. 13. Numbering of the surrounding vectors **s** and selection percentages for each surrounding vector $\{\mathbf{s}_i | 1 \leq i \leq 8N\}$. (a) The surrounding vector $\mathbf{s}_i$ is numbered clockwise starting from top left. (b) The percentages of the selected times versus the number of surrounding vectors $\mathbf{s}_i$ in Lena. When the line orientation in the block is vertical, $\mathbf{s}_9$ and $\mathbf{s}_{41}$ [the same blocks as $\mathbf{s}_N$ and $\mathbf{s}_S$ in Fig. 1(b)] are selected most frequently. Meanwhile, $\mathbf{s}_{25}$ and $\mathbf{s}_{57}$, which are the same blocks as $\mathbf{s}_E$ and $\mathbf{s}_W$ in Fig. 1(b), are mostly selected when the line orientation in the block is horizontal. Blocks $\mathbf{s}_{10}$, $\mathbf{s}_{25}$, $\mathbf{s}_{41}$, and $\mathbf{s}_{57}$ are selected more frequently when the line orientation is about $+45°$ (from top right to bottom left), and $\mathbf{s}_9$, $\mathbf{s}_{26}$, $\mathbf{s}_{39}$, and $\mathbf{s}_{57}$ are more frequently selected when the line orientation is about $-45°$ (from top left to bottom right).

TABLE II
MEAN AND VARIANCE OF ERROR FOR "LENA," "MASQUERADE," "PEPPERS," "BOAT," "ELAINE," AND "COUPLE" IN THE CASE OF 8×8 PIXEL BLOCK

		Ancis	Sun	Hemami	Shirani	Alkachouh	RIBMAP
Lena	mean	11.5	12.6	7.2	7.2	7.3	5.4
	variance	242.2	117.2	127.4	134.4	137.8	64.8
Masquerade	mean	18.6	15.6	12.7	12.8	12.3	10.0
	variance	437.9	276.2	313.3	336.4	290.7	184.3
Peppers	mean	12.4	12.3	7.7	7.7	7.4	5.9
	variance	290.9	126.6	121.2	126.9	91.3	69.3
Boat	mean	15.9	16.3	10.6	10.7	10.0	9.1
	variance	392.2	241.1	208.9	217.6	170.4	147.4
Elaine	mean	11.5	11.8	8.7	8.7	9.4	6.8
	variance	154.2	81.6	94.8	94.2	88.5	47.1
Couple	mean	12.2	14.4	8.4	8.4	7.3	7.2
	variance	264.2	186.7	185.7	184.6	165.1	143.6

To measure the usefulness of surrounding pixels, the selection percentage for each surrounding vector during the restoration process using the projection operator P_1 is used. As is shown in Fig. 13(a), each surrounding vector $\mathbf{s}_i$ is assigned indices from 1 to 64 clockwise starting at the top-left corner. The number of the selections for each surrounding vector in the projection operator P_1 is counted. Fig. 13(b) shows the percentages of the number of selections of each surrounding vector, $\{\mathbf{S}_k | 1 \leq k \leq 8N\}$. The result here shows that all surrounding vectors $\{\mathbf{S}_k | 1 \leq k \leq 8N\}$ are used during the restoration process.

To examine the reliability of the algorithms, the mean and variance of the error of the restored blocks in each image are calculated as $mean = (1/T) \sum_{m,n \in B_r} |f(m,n) - \hat{f}(m,n)|$ and $variance = (1/T) \sum_{m,n \in B_r} \{(f(m,n) - \hat{f}(m,n))^2\} - mean^2$ [25], where f is the original image, $\hat{f}$ is the restored image, B_r is the restored blocks in each image, and T is the total number of pixels in the restored blocks B_r. As shown in Table II, RIBMAP gives better results than the compared algorithms in both of mean and variance categories.

V. Conclusion

RIBMAP is a block-loss recovery algorithm based on projections for block-based image and video coding. Before applying the projection algorithm, proper recovery directions for missing blocks are first ascertained. From the initial set point, the spatial structure of neighborhood areas are expanded into the missing block. Two line masks are applied to determine the line orientation. With a block size of N, $8N$ pixel vectors are formed from the area surrounding the missing block. Two recovery vectors, consisting of both known and missing pixels, are introduced. Three convex sets are formulated to handle spatial information from the surrounding area of a lost block. Each recovery vector is alternately projected onto the lines and the convex sets. After missing pixels in each recovery vector are restored by these projections, new recovery vectors, including next missing pixels, are formulated. All missing pixels are, thereby, restored iteratively by alternating projections.

RIBMAP is tested on several standard images coded by JPEG and intracoding MPEG. In all cases, the reconstruction quality of RIBMAP is satisfactory and reliable and provides better restoration than competing methods when measured by the PSNR.

Acknowledgment

References

[1] *JPEG Tech. Spec., Revision 8, JPEG-8-R8*, ISO-IEC/JTC1/SC2/WP8, Aug. 1990.

[2] *ISO/IEC 13 818-2, Generic Coding of Moving Pictures and Associated Audio Information-Part 2: Video*, ISO/IEC 13 818-2 MPEG-2 Video Coding Standard, 1995.

[3] "Video codec for audiovisual services at $p \times 64$ kbits/s," CCITT Draft Revision of Recommendation H.261, CCITT SC XV, Description of Reference Model 8* RM8), Doc. 525, 1989.

[4] Y. Wang and Q. F. Zhu, "Error control and concealment for video communication: A review," in *Proc. IEEE Multimedia Signal Processing*, May 1998, pp. 974–997.

[5] Y. Wang, Q. F. Zhu, and L. Shaw, "Maximally smooth image recovery in transform coding," *IEEE Trans. Commun.*, vol. 41, no. 10, pp. 1544–1551, Oct. 1993.

[6] J. W. Park, J. W. Kim, and S. U. Lee, "DCT coefficients recovery-based error concealment technique and its application to the MPEG-2 bit stream error," *IEEE Trans. Circuits Syst. Video Technol.*, vol. 7, no. 8, pp. 845–854, Dec. 1997.

[7] X. Lee, Y.-Q. Zhang, and A. Leon-Garcia, "Information loss recovery for block-based image coding techniques-a fuzzy logic approach," *IEEE Trans. Image Process.*, vol. 4, no. 3, pp. 259–273, Mar. 1995.

[8] S. S. Hemami and T. H.-Y. Meng, "Transform coded image reconstruction exploiting interblock correlation," *IEEE Trans. Image Process.*, vol. 4, no. 7, pp. 1023–1027, Jul. 1995.

[9] S. Shirani, F. Kossentini, and R. Ward, "Reconstruction of baseline JPEG coded images in error prone environments," *IEEE Trans. Image Process.*, vol. 9, no. 7, pp. 1292–1299, Jul. 2000.

[10] Z. Alkachouh and M. G. Bellanger, "Fast DCT-based spatial domain interpolation of blocks in images," *IEEE Trans. Image Process.*, vol. 9, no. 4, pp. 729–732, Apr. 2000.

[11] H. Sun and W. Kwok, "Concealment of damaged blocks transform coded images using projections onto convex sets," *IEEE Trans. Image Process.*, vol. 4, no. 4, pp. 470–477, Apr. 1995.

[12] R. J. Marks II, "Alternating projections onto convex sets," in *Deconvolution of Images and Spectra*, P. A. Jansson, Ed. San Diego, CA: Academic, 1997, pp. 476–501.

[13] H. Stark and Y. Yang, *Vector Space Projections: A Numerical Approach to Signal and Image Processing, Neural Nets, and Optics*. New York: Wiley, 1998.

[14] D. C. Youla and H. Webb, "Image restoration by the method of convex projections: Part I-theory," *IEEE Trans. Med. Imag.*, vol. MI-1, no. 1, pp. 81–94, Jan. 1982.

[15] M. H. Goldburg and R. J. Marks II, "Signal synthesis in the presence of an inconsistent set of constraints," *IEEE Trans. Circuits Syst.*, vol. CAS-32, no. 4, pp. 647–663, Apr. 1985.

[16] D. C. Youla and V. Velasco, "Extensions of a result on the synthesis of signals in the presence of inconsistent constraints," *IEEE Trans. Circuits Syst.*, vol. CAS-33, no. 4, pp. 465–468, Apr. 1986.

[17] S. Oh, R. J. Marks, and L. E. Atlas, "Kernel synthesis for generalized time-frequency distributions using he method of alternating projections onto convex sets," *IEEE Trans. Signal Process.*, vol. 42, no. 7, pp. 1653–1661, Jul. 1994.

[18] R. Gonzalez and R. Woods, *Digital Image Processing*. Reading, MA: Addison-Wesley, 1992.

[19] S. Tsekeridou and I. Pitas, "MPEG-2 error concealment based on block-matching principles," *IEEE Trans. Circuits Syst. Video Technol.*, vol. 10, no. 4, pp. 646–658, Jun. 2000.

[20] Y. Yang, N. P. Galatsanos, and A. K. Katsaggelos, "Projection-based spatially adaptive reconstruction of block transform compressed images," *IEEE Trans. Image Process.*, vol. 4, no. 7, pp. 896–908, Jul. 1995.

[21] Y. Yang and N. P. Galatsanos, "Removal of compression artifacts using projections onto convex sets and line process modeling," *IEEE Trans. Image Process.*, vol. 10, no. 10, pp. 1345–1357, Oct. 1997.

[22] M. Ancis and D. D. Giusto, "Reconstruction of missing blocks in JPEG picture transmission ," in *Proc. IEEE Pacific Rim Conf.*, Aug. 1999, pp. 288–291.

[23] A. S. Tom, C. L. Yeh, and F. Chu, "Packet video for cell loss protection using deinterleaving and scrambling," in *Proc. Int. Conf. Acoustics, Speech, and Signal Processing*, Toronto, ON, Canada, May 1991, pp. 2857–2860.

[24] A. Gersho and R. Gray, *Vector Quantization and Signal Compression*. Norwell, MA: Kluwer, 1992.

[25] A. Papoulis, *Probability, Random Variables, and Stochastic Processes*. New York: McGraw-Hill, 1984.

Jiho Park (M'93) received the Ph.D. degree in electrical engineering from the University of Washington, Seattle, in 2002. His Ph.D. research involved error-resilient image/video communications and post-processing error concealment.

He joined Samsung Electronics Communication Research Laboratories in 2002. He is currently working on video and multimedia signal precessing and communications. His current interests include video and signal processing, joint source and channel coding, pattern recognition, and communications.

Dong-Chul Park (S'80–M'90–SM'99) received the B.S. degree in electronics engineering from Sogang University, Seoul, Korea, in 1980, the M.S. degree in electrical and electronics engineering from the Korea Advanced Institute of Science and Technology, Seoul, in 1982, and the Ph.D. degree in electrical engineering, with a dissertation on system identification using neural networks, from the University of Washington (UW), Seattle, in 1990.

From 1990 to 1994, he was with the Department of Electrical and Computer Engineering, Florida International University, The State University of Florida, Miami. Since 1994, he has been with the Department of Information Engineering, MyongJi University, Korea, where he holds the title of Professor. From 2000 to 2001, he was a Visiting Professor at UW. He is a pioneer in the area of electric load forecasting using neural networks. He has published more than 50 papers, including 20 archival journals in the area of neural network (NN) algorithms and their applications. His current interests include the development of NN algorithms and their applications to various engineering problems, including financial engineering, image compression, speech recognition, and pattern recognition. He is the founder of NeuroSolutions, Co., Korea, where he develops IT solutions, including fraud detection system for credit card business.

Dr. Park was a member of the Editorial Board for the IEEE TRANSACTIONS ON NEURAL NETWORKS from 2000 to 2002.

Mohamed A. El-Sharkawi (F'95) received the B.Sc. degree in electrical engineering from the Cairo High Institute of Technology, Cairo, Egypt, in 1971 and the M.A.Sc. and Ph.D. degrees in electrical engineering from the University of British Columbia, Vancouver, BC, Canada, in 1977 and 1980, respectively.

In 1980, he joined the University of Washington, Seattle, where he is presently a Professor of electrical engineering. He is the Founder of the International Conference on the Application of Neural Networks to Power Systems (ANNPS) and a Co-Founder of the International Conference on Intelligent Systems Applications to Power (ISAP). He is a current or past member of the editorial boards or Associate Editor of several journals. He is the author of a textbook on *Fundamentals of Electric Drives* (Pacific Grove, CA: Brooks Cole, 2000). He has organized and taught several international tutorials on intelligent systems applications, power quality, and power systems, and has organized and chaired numerous panel and special sessions in international conferences. He has published over 160 papers and book chapters in these areas and holds five licensed patents.

Dr. El-Sharkawi is the Editor and Co-Editor of several IEEE tutorial books on the applications of intelligent systems. He is the Vice President for technical activities of the IEEE Neural Networks Society. He is a founding Chairman of several IEEE task forces, working groups, and subcommittees.

Robert J. Marks II (F'94) holds the position of Distinguished Professor of Electrical and Computer Engineering, Department of Engineering, Baylor University, Waco, TX. He has over 250 publications. He is the author and coauthor of the books *Introduction to Shannon Sampling and Interpolation Theory* (New York: Springer-Verlag, 1991), and *Neural Smithing: Supervised Learning in Feedforward Artificial Neural Networks* (Cambridge, MA: MIT Press, 1999). He is a Co-Editor of five other volumes. He was also the Topical Editor for Optical Signal Processing and Image Science for the *Journal of the Optical Society of America A*.

Prof. Marks is a Fellow of the Optical Society of America. He was awarded the Outstanding Branch Counselor award by the IEEE and the IEEE Centennial Medal. He was named a Distinguished Young Alumnus of the Rose-Hulman Institute of Technology and is an inductee into the Texas Tech Electrical Engineering Academy. In 2000, he was awarded the Golden Jubilee Award by the IEEE Circuits and Systems Society. He is also the first recipient of the IEEE Neural Networks Society Meritorious Service Award. He was given the honorary title of Charter President of the IEEE Neural Networks Council. He served as an IEEE Distinguished Lecturer. He served a six-year term as the Editor-in-Chief of the IEEE TRANSACTIONS ON NEURAL NETWORKS and as an Associate Editor of the IEEE TRANSACTIONS ON FUZZY SYSTEMS. He serves as the Administrative Vice President of the IEEE Circuits and Systems Society.